World Academy of Science, Engineering and Technology
International Journal of Environmental and Ecological Engineering
Vol:9, No:1, 2015

Turbulence Modeling and Wave-Current Interactions

A.-C. Bennis, F. Dumas, F. Ardhuin, B. Blanke

Abstract—The mechanics of rip currents are complex, involving interactions between waves, currents, water levels and the bathymetry, that present particular challenges for numerical models. Here, the effects of a grid-spacing dependent horizontal mixing on the wave-current interactions are studied. Near the shore, wave rays diverge from channels towards bar crests because of refraction by topography and currents, in a way that depends on the rip current intensity which is itself modulated by the horizontal mixing. At low resolution with the grid-spacing dependent horizontal mixing, the wave motion is the same for both coupling modes because the wave deviation by the currents is weak. In high resolution case, however, classical results are found with the stabilizing effect of the flow by feedback of waves on currents. Lastly, wave-current interactions and the horizontal mixing strongly affect the intensity of the three-dimensional rip velocity.

Keywords—Numerical modeling, Rip currents, Turbulence modeling, Wave-current interactions.

I. Introduction

RIP currents are the main subject of several studies since the pioneer work of [1]. The reasons include the ability of rip currents to move large volumes of water and sediment. Furthermore, rip currents sweep away many swimmers each year causing more casualties than hurricanes as well as severe storms in places like Florida [2] or on the French coasts where currents are a key factor in 126 of the deadly drownings reported for the year 2012 [3]. From observations taken on the beach of La Jolla in California, [4] described the rip structure as being composed of three major features: the feeder, the neck and the head. Scientific studies started by qualitative description based on observations. Then, some theoretical and numerical approaches have been developed for rip currents, using the observations for validation.

The mechanism of rip current generation differs according to the authors. Some of them think that rip currents are the result of a hydrodynamic instability resulting from wave refraction by currents ([5], [6], [7]), but other effects can be important such as the convergence of longshore currents in regions of strong alongshore variations in wave conditions [8]. The main numerical studies considering the currents effects on waves (hereafter CEW) report the following behaviors: a) [5] observed a modification of the flux of wave energy by the currents, with variability along the longshore coordinate, b) [9] found that CEW reduces the offshore extent of rip currents, c) [10] showed that rips are compacted with CEW because of a strong decrease of the wave flux of momentum because of wave breaking. They explained that this decrease is due to the change in wave number (wave ray bending), d) [11] complemented the latter study by calculating the change in the wavefield resulting from wave ray bending and from the current flux of wave energy. They express the wave-current interactions in terms of bottom friction.

All previous studies investigating the currents effects on waves were carried out without turbulence modeling and at high resolution: 2 and 3 meters in both horizontal directions for [11] and [10], respectively. Unfortunately, these operating conditions are not always available, in particular to simulate in-situ experiments. Unstructured meshes with refinements near the shore and multigrid methods are generally employed to sample the maximum of scales with the minimum cost. As horizontal and vertical mixing must be modeled in such conditions, it is essential to understand the impact of turbulence modeling on the wave-current interactions.

We choose to study the sensitivity of the rip system to horizontal mixing. We continue the bi-dimensional work of [11] with three-dimensional (3D) simulations. We use the vortex force formalism ([12], [13]). Our work provides new knowledge about the following points: a) CEW impact is modulated by the horizontal mixing, with maximum effects at high resolution when a grid-spacing dependent parameterization is used ; b) the divergence of the waves from the peak of the bar depends on the rip intensity which is itself modulated by the mixing.

The outline of the paper is as follows. The methodology including the governing equations and details about the experiments is described in Section II. Results are presented in Section III. We summarize our

A.-C. Bennis is with M2C, UCBN-CNRS-UR, 24 rue des Tilleuls, 14000 Caen, France (corresponding author to provide phone: +33231565718 ; fax: +33231565757 ; e-mail: anne-claire.bennis@unicaen.fr).

F. Dumas is with Dyneco/Physed, Ifremer, Technopole Pointe du diable, 29280 Plouzane, France (e-mail: franck.dumas@ifremer.fr).

F. Ardhuin was with LOS (Ifremer). He is now with LPO, CNRS-UBO-IRD-Ifremer, Technopole Pointe du diable, 29280 Plouzane, France (e-mail: fabrice.ardhuin@ifremer.fr).

B. Blanke is with LPO, CNRS-UBO-IRD-Ifremer, Avenue Victor Le Gorgeu, 29200 Brest, France (e-mail: bruno.blanke@univ-brest.fr).

findings in Section IV.

II. Methodology

The 3D fully coupled MARS-WAVEWATCH III model (more details in [13] and [14]) combines the MARS3D hydrodynamic model [15] and the WAVEWATCH III wave model [16], hereafter WW3. The exchanges between the models are managed by the PALM coupler [17]. We can easily investigate the feedback of currents on waves by turning off the coupling in test simulations. All the results presented here come from a non stationary coupling procedure.

WW3 is a phase-averaged wave model. The wave action density spectrum N (N being a function of time, space, wave number and direction) is solved:

$$\frac{DN}{Dt} = \frac{S}{\sigma} \tag{1}$$

where S represents the total source term, including non-linear interactions, bottom friction, wave dissipation and bottom scattering (more details in [16] and [18]). σ is the intrinsic wave radian frequency. High-order conservative numerical schemes are used for spatial discretization. A CFL (Courant-Friedrichs-Lewy) condition exists, binding the discretizations in time and in space.

MARS3D uses the pressure projection method to solve the 3D, unsteady, Navier-Stokes equations under the Boussinesq and hydrostatic assumptions. Finite difference schemes are used for the spatial discretization performed on an Arakawa-C grid [15]. The model uses an ADI (Alternate Direction Implicit) time scheme [19]. However, the time step of MARS3D is constrained by the CFL condition of WW3 in order to avoid a too large time shift between both models.

Fig. 1 sketches the problem geometry and computational domain. Since we are concerned in rip currents, the rip channels are near the center of the domain and periodic boundary conditions are used at the lateral boundaries. Neumann boundary conditions are employed at the surface and at the bottom, with the additional use of the parameterization of [20] for bottom friction [14]. Offshore, open boundary conditions based on the method of characteristics are applied. The effects of wave breaking on mixing are accounted with the boundary conditions of [21] for turbulent quantities at the surface.

The flow is forced by the normal propagation of an incident wave on a barred beach. Each case uses a regular horizontal grid. The time step varies according to the mesh to ensure the convergence of the wave model and the time synchronization of the coupled system. The coupling time step is also different from the time step of both models (see Table I).

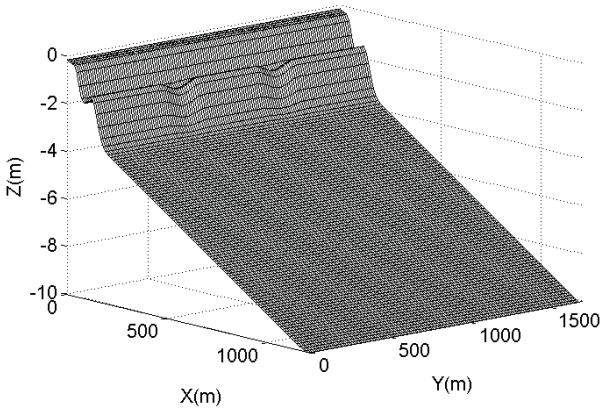

Fig. 1 Bathymetry

A. Governing Equations

Wave forcing has been implemented into the hydrodynamic model with the vortex force method ([22], [12]). This method has been validated for surf zone cases (e.g. [23], [24] and [14]) and gives good agreement with in-situ and laboratory data. The main advantage of the method is to consider the mean flow instead of the total momentum ([12], [13]), allowing us to produce realistic results by avoiding the delicate problem of the modeling of the vertical flux of momentum.

The equations of motion for a wave-forced, 3D, incompressible, unsteady, hydrostatic, constant-density flow are given in [12] and [13]. Their generic formulation is:

$$\begin{aligned} \frac{\mathrm{D}\mathcal{U}}{\mathrm{Dt}} &= \mathbf{S_{EPG}} + \mathbf{S_{VM}} + \mathbf{S_{HM}} + \mathbf{S_{WP}} \\ &+ \mathbf{S_{BA}} + \mathbf{S_{BBL}} + \mathbf{S_{VF}} \end{aligned} \tag{2}$$

where $\mathcal{U} = (U, V, W)$ is the 3D quasi-Eulerian velocity computed as the Lagrangian velocity minus the Stokes drift. The source terms $\mathbf{S_{EPG}}$, $\mathbf{S_{VM}}$, $\mathbf{S_{HM}}$, $\mathbf{S_{BA}}$, $\mathbf{S_{BBL}}$, $\mathbf{S_{VF}}$, $\mathbf{S_{WP}}$ are related to: the external pressure gradient, the vertical mixing, the horizontal mixing, the breaking acceleration, the streaming, the vortex force and the wave-induced pressure gradient, respectively. These equations are similar to the ones of [22] used in [25] and [23].

The k-ϵ scheme, modified according to [26], is used to model the vertical mixing. Horizontal mixing is decomposed into two components: the scheme of [27] and a diffusion term that is either taken constant or grid-spacing dependent like in [28]. So, we have:

$$S_{HM,x} = \frac{1}{\rho}\left(\frac{\partial\left(\rho\nu_H\frac{\partial U}{\partial x}\right)}{\partial x} + \frac{\partial\left(\rho\nu_H\frac{\partial U}{\partial y}\right)}{\partial y}\right) \quad (3)$$

$$S_{HM,y} = \frac{1}{\rho}\left(\frac{\partial\left(\rho\nu_H\frac{\partial V}{\partial x}\right)}{\partial x} + \frac{\partial\left(\rho\nu_H\frac{\partial V}{\partial y}\right)}{\partial y}\right) \quad (4)$$

where $S_{HM,x}$ and $S_{HM,y}$ are the cross-shore and alongshore components of $\mathbf{S_{HM}}$, respectively. ρ is the water density.

ν_H is the horizontal viscosity:

$$\nu_H = \nu_1 + \nu_2 \quad (5)$$

where $\nu_1 = f_{visc}\cdot 0.01\cdot(\Delta_{xy})^{1.15}$ (Δ_{xy} is the grid spacing, f_{visc} is a user-defined parameter, set to 10 here) [15]. ν_2 is the Battjes's term (more details in [27]).

B. Experiments

We aim at studying the dependence of the flow response on horizontal mixing. Both coupling modes will be compared. The bedform is an approximation of the beach profile measured at Duck, North Carolina, on October 11, 1990 (see Fig. 1). Its analytical expression, $h(x,y)$, was given by [10] as:

$$\begin{aligned} h_0(x) &= \left(a_1 - \frac{a_1}{\gamma_1}\right)\tanh\left(\frac{b_1 x}{a_1}\right) \\ &+ \frac{b_1 x}{\gamma_1} - a_2\exp\left[-5\left(\frac{x-x_c}{x_c}\right)^2\right] \end{aligned} \quad (6)$$

where $x_c = 80\,\mathrm{m}$ is the location of the longshore bar. γ_1, a_1, b_1 and a_2 are set to 11.74, 2.97 m, 0.075, 1.5 m, respectively. Adding a perturbation at the longshore bar, the following bottom profile is obtained:

$$h(x,y) = h_0(x) + h_1(x,y) \quad (7)$$

with

$$h_1(x,y) = h_0(x)\epsilon\cos\left(\frac{2\pi y}{\lambda}\right)\exp\left[-5\left(\frac{x-x_c}{x_c}\right)^2\right] \quad (8)$$

where $\epsilon = 0.1\,\mathrm{m}$ and $\lambda = 256\,\mathrm{m}$ are the magnitude and the wavelength of the perturbation, respectively.

A Gaussian wave spectrum is used at the offshore boundary. [11] preferred to use the JONSWAP spectrum, but this choice has only little impact on our conclusions. The offshore wave characteristics are detailed in Table I.

Five cases (A(1), A(2), B(1), B(2) and C(1,2)) are carried out. They differ by their horizontal resolution, from 3 to 24 meters, and by their horizontal mixing (see Tables II and III). The grid spacing and time steps for these configurations are summarized in Table III. We use 15 sigma levels over the vertical. Both coupling modes use the same set of parameters to ensure a comparison as clean as possible. For each resolution, some sensitivity tests on mixing are carried out, with variable ν_1 (see Table II). When $\mathrm{f_{visc}} = 10$, with a resolution of 3 meters, ν_1 is about $0.3\,m^2.s^{-1}$. So, we have only the case C(1,2) at this resolution.

TABLE I: COMMON CHARACTERISTICS of ALL SIMULATIONS (SI UNITS ARE: m = METER, ° = DEGREE, s = SECOND)

Characteristic	Value
Wave height	$H_s = 1\,\mathrm{m}$
Wave period	$T = 10\,\mathrm{s}$
Wave direction	$\theta = 90°$
Magnitude of perturbation	$\epsilon = 0.1$
Spacing of rip channels	$\lambda = 256\ \mathrm{m}$

TABLE II: LIST of TEST CASES for DIFFERENT SPATIAL RESOLUTIONS and HORIZONTAL MIXING FORMULATIONS (SI UNITS ARE: m = METER and s = SECOND).

Case	i) ν_1 is computed with $\mathrm{f_{visc}} = 10$ ii) ν_2 is unchanged	i) $\nu_1 = 0.3\,\mathrm{m^2.s^{-1}}$ ii) ν_2 is unchanged
A	A(1)	A(2)
B	B(1)	B(2)
C	C(1,2)	C(1,2)

TABLE III: GRID SPACING and TIME STEPS for ALL CASES. Δ_{XY} IS THE GRID SPACING IN BOTH HORIZONTAL DIRECTIONS. $\Delta\mathrm{T_W}$ and $\Delta\mathrm{T_M}$ ARE THE MODEL TIME STEPS for WW3 and MARS3D, RESPECTIVELY. $\Delta\mathrm{T_C}$ IS THE COUPLING TIME STEP. (SI UNITS ARE: m = METER and s = SECOND).

Case	Δ_{xy}	$\Delta\mathrm{T_W}$	$\Delta\mathrm{T_M}$	$\Delta\mathrm{T_C}$
A: A(1), A(2)	24 m	0.5 s	1 s	1 s
B: B(1), B(2)	12 m	0.33 s	1 s	1 s
C: C(1,2)	3 m	0.15 s	0.5 s	1 s

III. Results

We investigate the impact of the formulation used for horizontal mixing on the wave-current interactions. We study in particular grid-spacing dependent formulation: ν_2 is unchanged while different values for ν_1 are tested.

Unlike the wave number, the wave height is little affected by the coupling mode in all runs. Because of mixing the rip currents are weak and, therefore, they have a limited effect on wave shoaling. At low resolution, and for both horizontal mixing cases (A(1) and A(2)), the effects of rip currents on the wave height vanish.

The changes in wave number ascribed to CEW are shown in Fig. 2. The wave number increases near the coast because of the refraction processes that deviate the incident normal wave. Equivalent results are obtained in all runs. Refraction is only due to bottom topography in the case WEC-only. When CEW is activated, waves are also refracted by the currents. So, the changes in wave number are larger with CEW+WEC compared to WEC-only (see Fig. 2). The wave number is only slightly modified by both horizontal mixing and grid spacing in the case WEC-only because only bottom topography causes refraction. In contrast, the grid-spacing dependent horizontal mixing modifies the WEC+CEW simulations (i.e., C(1,2) vs. A(1)). At high resolution (i.e., C(1,2)), the increase in wave number ascribed to the currents is about 2.5 times greater than at low resolution with the grid-spacing dependent horizontal mixing (i.e., A(1)). The mixing is stronger at low resolution because of its formulation and, therefore, the rip currents are weaker. As a result, they have less impact on the wave field. The comparison of A(1) and A(2) shows a maximal change in wave number in A(2) for which the mixing is the weakest.

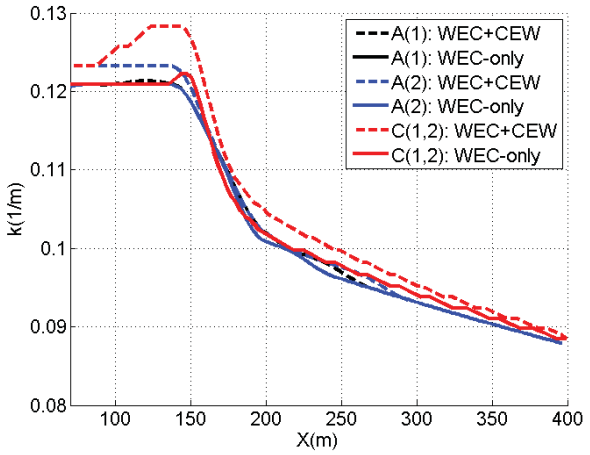

Fig. 2 Cross-shore profiles of the wave number inside the rip channel for the cases A(1), A(2) and C(1,2) and for both coupling cases at t = 140 min.

[11] also investigated the sensitivity to CEW in their simulations. For this purpose, they calculated the change in wave number for both horizontal directions (Δk_x and Δk_y, respectively)

$$\Delta k_x \simeq -\left\langle \frac{k}{\sigma} \right\rangle \Delta\sigma \quad \text{and} \quad \Delta k_y \simeq \int_x^{LY} \left\langle \frac{k}{\sigma} \right\rangle \frac{\partial(\Delta\sigma)}{\partial y} dx' \tag{9}$$

where the Δ operator refers to the difference ascribed to CEW, σ is the intrinsic wave radian frequency, k is the wave number and LY is the alongshore width.

The Doppler shift $\Delta\sigma$ is computed as

$$\Delta\sigma = \sigma^{WEC+CEW} - \sigma^{WEC-only} \tag{10}$$

In contrast with their study, our Doppler shift is positive everywhere. As expressed by their (13), the Doppler shift is a function of the cross-shore velocity and of the alongshore mean of the wave number. Our rip currents being weaker everywhere, the onshore flow is too weak to produce negative Doppler shifts. A positive doppler shift is obtained in all cases because it depends on the rip intensity which is itself by the horizontal mixing.

Fig. 3 shows the alongshore group velocity (C_{g_y}) for the cases A(1), A(2) and C(1,2). C_{g_y} is non zero, in all runs, only at locations near the shore (between $x = 50\,\mathrm{m}$ and $x = 120\,\mathrm{m}$). When CEW is activated, C_{g_y} is weaker than for the case WEC-only because of the interactions with currents. From offshore to onshore, waves are first deviated by the currents, second by the bottom topography. For the case A(1), where a grid-spacing dependent horizontal mixing is used (Fig. 3, top row), the refraction by the currents is almost negligible and occurs only near the shore. In contrast, the waves are significantly deviated by the rip current in the case A(2) where a weaker mixing is applied (Fig. 3, middle row). However, the patterns seem more diffuse than for the case C(1,2) where the same value is used for the horizontal mixing. This is probably due to the coarser description of the bathymetry at low resolution. Deviations by the currents are expressed by the convergence of the alongshore group velocity to the rip channel on the offshore side of the wave motion. Near the shore, the waves diverge away from the rip channels towards the bar (Fig. 4, black arrows). Indeed, refractions by current and by topography produce, at a given alongshore location, C_{g_y} values with opposite signs. [11] obtained a different result, with wave convergence towards the rip channels because their C_{g_y} values caused by all the refraction processes have the same sign at a given alongshore location. Their rip currents have an intensity twice larger than ours and, therefore, the refraction by rip currents is more significant than the refraction by bottom topography.

The cross-shore profiles of the barotropic cross-shore velocity, for the cases A(1), A(2), B(1), B(2) and C(1,2) and for all coupling modes, are presented in Fig. 5. For a same value of the horizontal mixing (bottom row), the cross-shore profiles are similar at all resolutions and for each coupling case because the all numerical schemes are conservative. Some differences are observed with a grid-spacing dependent mixing, in particular for the case

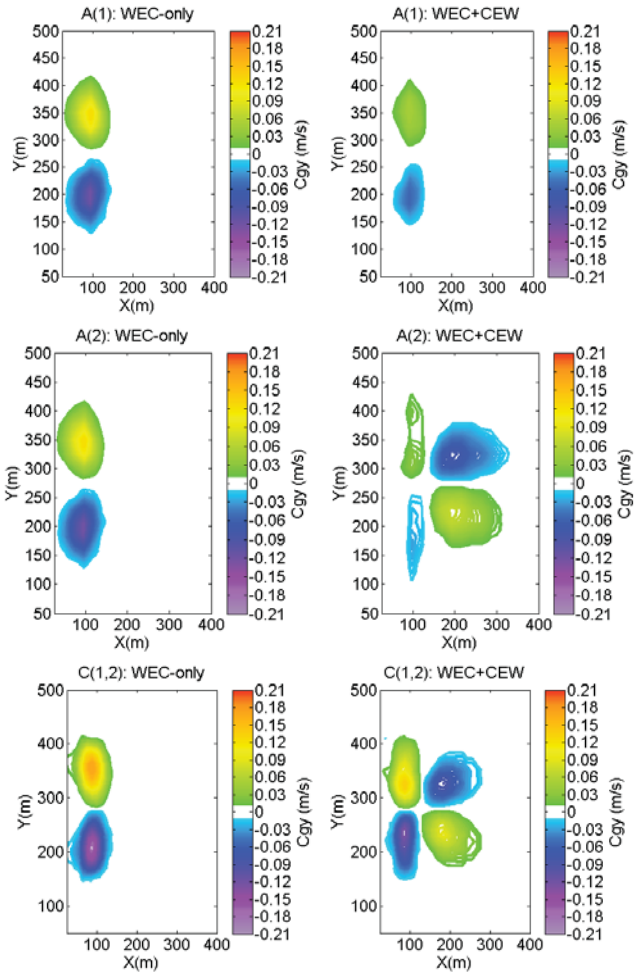

Fig. 3 C_{g_y} for the cases WEC-only and WEC+CEW shown on the left- and right-hand sides, respectively. Cases A(1) (top), A(2) (middle) and C(1,2) (bottom) are displayed. Contours are equally spaced from -0.21 m.s^1 to 0.21 m.s^1. All figures are plotted at $t = 140$ min

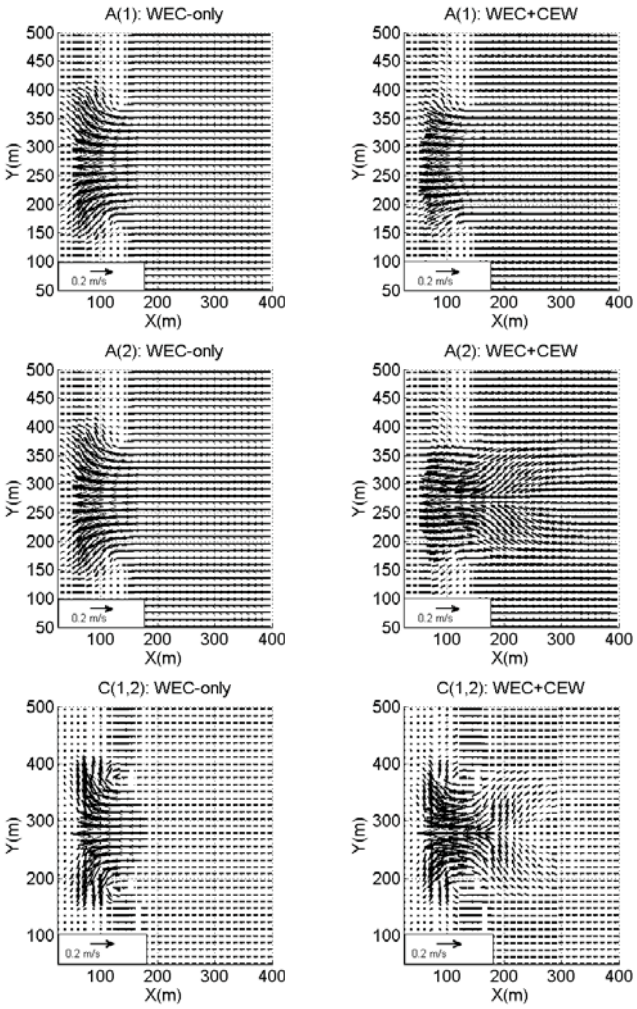

Fig. 4 Alongshore perturbation of the group velocity (black arrows) for the cases WEC-only and WEC+CEW shown on the left- and right-hand sides, respectively. Cases A(1) (top), A(2) (middle) and C(1,2) (bottom) are displayed. Arrows are plotted on a 12 m stencil. All figures are plotted at $t = 140$ min.

WEC-only (top row). As the mixing is increased with the grid spacing, the flow at low resolution is smoother than at high resolution. The offshore extension is significantly reduced by CEW as expected for the finest grid. We note that the reduction is very weak at low resolution. At $x = 300\,\mathrm{m}$, the WEC+CEW barotropic cross-shore velocity for the case C(1,2) is about $0.07\,\mathrm{m/s}$ whereas it reaches $0.15\,\mathrm{m/s}$ for WEC-only. We have a factor of two between both velocities. The more the grid spacing is increased, the more this factor is decreased. As the feedback stabilize the flow, the barotropic velocities are almost independent the horizontal mixing.

Fig. 6 presents x-z maps of the 3D quasi-Eulerian cross-shore velocity (U) for the cases A(1), B(1), C(1,2) and for all coupling modes. A(2) and B(2) are not shown because the vertical profiles are the same since the simulations use similar horizontal mixing. As in [23], the maximum of the rip velocity is located within the water column. The rip current decreases towards the bottom and the surface. The shear of the rip velocity is only slightly modified by the feedback. The vertical profiles are close for both coupling modes for the case A(1), while large differences are observed for the case C(1,2), which confirms our conclusions drawn from the profiles of the barotropic velocity. These differences are ascribed to the horizontal mixing, which is more intense for the case A(1). At $x = 300\,\mathrm{m}$ and for the case C(1,2), the WEC-only maximum velocity is about 1.8 times the one found for WEC+CEW. The small differences between the cases with CEW stem for a degraded description of the bathymetry at low resolution.

IV. Summary and Conclusions

Rips currents are investigated with a 3D fully coupled wave-current model. We consider horizontal

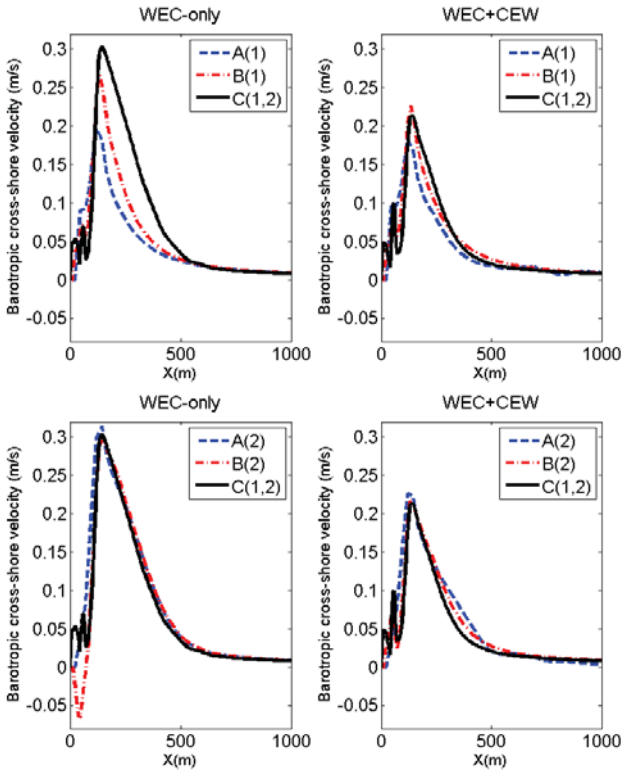

Fig. 5 Cross-shore profiles of the barotropic quasi-Eulerian cross-shore velocity inside the rip channel: A(1), B(1) and C(1,2) at the top; A(2), B(2) and C(1,2) at the bottom. WEC-only and WEC+CEW cases are shown on the left- and right-hand sides, respectively. All figures are plotted at $t = 140$ min.

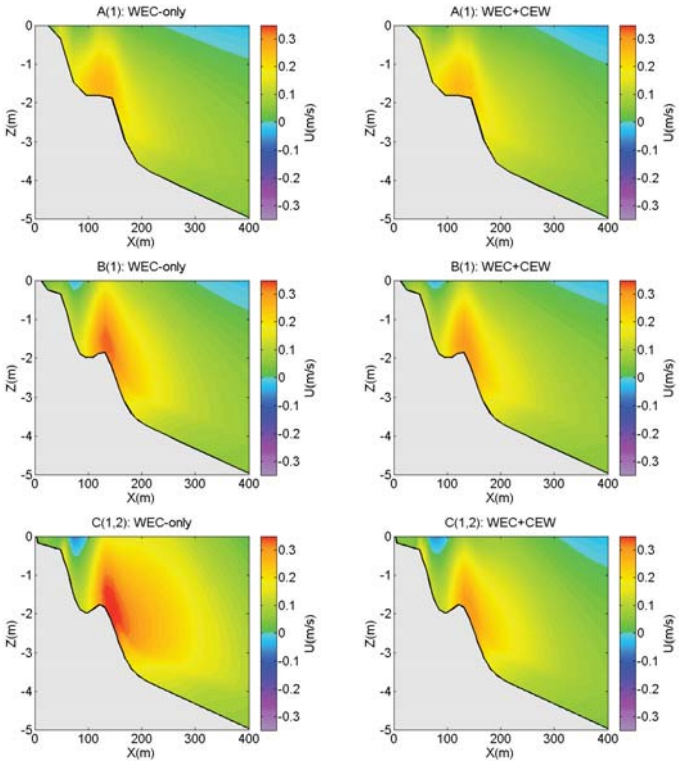

Fig. 6 x-z maps of the 3D quasi-Eulerian cross-shore velocity for the cases A(1) (top), B(1) (middle) and C(1,2) (bottom), inside the rip channel. The WEC-only and WEC+CEW cases are shown from left to right. Contours are equally spaced from -0.35 m.s^1 to 0.35 m.s^{-1}. All figures are plotted at $t = 140$ min.

resolutions from 3 to 24 meters. Several horizontal mixing formulations are tested and the simulations are performed for both coupling modes.

We test the impact of a grid-spacing dependent horizontal mixing on the wave-current interactions. At low resolution and for all mixing cases, the effects of rip currents on the wave height vanish. The Doppler shift due to refraction by currents is modified by the horizontal mixing. In contrast with the study of [11], we find in all runs a Doppler shift that is everywhere positive. This result stems from our rip velocity that is weaker than in their paper because of the values we use here for horizontal mixing. Consequently, the change in the alongshore group velocity is different: the change in C_{g_y} ascribed to CEW is not sufficient to deviate waves to the channel, which shows that this deviation is modulated by the horizontal mixing. Here, the refraction by the bottom topography drives the wave motion near the shore. As a result, the waves diverge away from the rip channels toward the peak of the bar instead of converging towards the rip channels. Furthermore, when a grid-spacing dependent mixing is used, a high resolution is necessary to observe significant effects ascribed to CEW. When a same value of horizontal mixing is taken, the 3D and depth-averaged velocity profiles are almost independent of the spatial resolution for all coupling modes. In contrast, with a grid-spacing dependent horizontal mixing, the WEC-only velocity is modified by the spatial resolution. The peak velocity and the offshore extension of the current are accentuated by a decrease in grid spacing. In all cases the flow becomes almost independent of the horizontal resolution when CEW is activated because of its ability to stabilize the flow.

To conclude, the horizontal mixing is found to have direct impacts on the wave-current interactions. We show that the conclusions of [11] and [10] depend on the horizontal mixing. This result is important because the wave-current models are also used to simulate coastal seas where the mixing is taken into account. Indeed, direct numerical simulations (i.e. without turbulence modeling) are too expensive to simulate the flow at these scales because of the larger size of the computational domain.

ACKNOWLEDGMENTS

A-C. B. acknowledges the support of a post-doctoral grant from Université de Bretagne Occidentale, the PREVIMER and IOWAGA projects. A-C. B. is also supported by the University of Caen. F.D. is supported by Ifremer and the PREVIMER project. F.A. is supported by a FP7-ERC grant #240009 IOWAGA, Ifremer and CNRS. B.B. is supported by CNRS.

REFERENCES

[1] F. P. Shepard, "Undertow, rip tide or rip current," *Science*, vol. 84, pp. 181–182, 1936.

[2] J. H. MacMahan, E. B. Thornton, and A. J. Reniers, "Rip current review," *Coastal Eng.*, vol. 53, pp. 191–208, 2006.

[3] L. Lasbeur and B. Thelot, "Epidemiological surveillance of drowning - the noyades 2012 survey. 1 june-30 september 2012," Saint Maurice: Institut de veille vanitaire, Tech. Rep., 2013.

[4] F. P. Shepard, K. O. Emery, and E. C. L. Fond, "Rip currents: A process of geological importance," *Journal of Geology*, vol. 49, pp. 337–369, 1941.

[5] P. H. Leblond and C. L. Tang, "On energy coupling between waves and rip currents," *J. Geophys. Res.*, vol. 79, pp. 811–816, 1974.

[6] A. Falques, A. Montoto, and D. Vila, "A note on hydrodynamic instabilities and horizontal circulation in the surf zone," *J. Geophys. Res.*, vol. 104, no. C9, pp. 20 605–20 615, 1999.

[7] J. Yu, "On the instability leading to rip currents due to wave-current interaction," *J. Fluid Mech.*, vol. 549, pp. 403–428, 2006.

[8] J. W. Long and H. T. Ozkan-Haller, "Offshore controls on nearshore rip currents," *J. Geophys. Res.*, vol. 110, p. C12007, 2005.

[9] K. A. Haas, I. A. Svendsen, and M. C. Haller, "Numerical modeling of nearshore circulations on a barred beach with rip channels, paper presented at the 26th conference on coastal engineering," *Am. Soc. of Civ. Eng.*, 1998.

[10] J. Yu and D. N. Slinn, "Effects of wave-current interaction on rip currents," *J. Geophys. Res.*, vol. 108, no. C3, p. 3088, 2003.

[11] B. Weir, Y. Uchiyama, E. M. Lane, J. M. Restrepo, and J. C. McWilliams, "A vortex force analysis of the interaction of rip currents and surface gravity waves," *J. Geophys. Res.*, vol. 116, p. C05001, 2011.

[12] F. Ardhuin, N. Rascle, and K. A. Belibassakis, "Explicit wave-averaged primitive equations using a generalized Lagrangian mean," *Ocean Modelling*, vol. 20, pp. 35–60, 2008.

[13] A.-C. Bennis, F. Ardhuin, and F. Dumas, "On the coupling of wave and three-dimensional circulation models: Choice of theoretical framework, practical implementation and adiabatic tests," *Ocean Modelling*, vol. 40, pp. 260–272, 2011.

[14] A.-C. Bennis, F. Dumas, F. Ardhuin, and B. Blanke, "Mixing parameterization: impacts on rip currents and wave set-up," *Ocean Engineering*, vol. 42, pp. 213–227, 2014.

[15] P. Lazure and F. Dumas, "An external-internal mode coupling for a 3d hydrodynamical model for applications at regional scale (MARS)," *Adv. Water Resources*, vol. 31, pp. 233–250, 2008.

[16] H. L. Tolman, "User manual and system documentation of WAVEWATCH-III^{TM} version 3.14," NOAA/NWS/NCEP/MMAB, Tech. Rep. 276, 2009.

[17] S. Buis, A. Piacentini, and D. Déclat, "PALM: A computational framework for assembling high performance computing applications," *Concurrency Computat.: Pract. Exper.*, vol. 18, no. 2, pp. 247–262, 2008.

[18] F. Ardhuin, E. Rogers, A. Babanin, J.-F. Filipot, R. Magne, A. Roland, A. van der Westhuysen, P. Queffeulou, J.-M. Lefevre, L. Aouf, and F. Collard, "Semi-empirical dissipation source functions for wind-wave models: part i, definition, calibration and validation," *J. Phys. Oceanogr.*, vol. 40, pp. 1917–1941, 2010.

[19] A. Bourchtein and L. Bourchtein, "Modified time splitting scheme for shallow water equations," *Mathematics and Computers in Simulation*, vol. 73, pp. 52–64, 2006.

[20] R. L. Soulsby, "Bed shear stresses due to combined waves and currents. In: Stive, M., Fredsøe, J., Hamm, L., Soulsby, R., Teisson, C., Winterwerp, J. (Eds)," *Advances in Coastal Morphodynamics, Delft Hydraulics, Delft, The Netherlands*, pp. 420–423, 1995.

[21] H. Burchard, "Simulating the wave-enhanced layer under breaking surface waves with two-equation turbulence models," *J. Phys. Oceanogr.*, vol. 31, pp. 3133–3145, 2001.

[22] J. C. McWilliams, J. M. Restrepo, and E. M. Lane, "An asymptotic theory for the interaction of waves and currents in coastal waters," *J. Fluid Mech.*, vol. 511, pp. 135–178, 2004.

[23] N. Kumar, G. Voulgaris, J. C. Warner, and M. Olabarrieta, "Implementation of the vortex force formalism in the coupled ocean-atmosphere-wave-sediment transport (COAWST) modeling system for inner shelf and surf zone applications," *Ocean Modelling*, vol. 47, pp. 65–95, 2012.

[24] S. Moghimi, K. Klingbeil, U. Grawe, and H. Burchard, "A direct comparison of the depth-dependent radiation stress method and a vortex force formulation within a three-dimensional ocean model," *Ocean Modelling*, pp. 1–38, 2012.

[25] Y. Uchiyama, J. C. McWilliams, and A. F. Shchepetkin, "Wave-current interaction in oceanic circulation model with a vortex-force formalism Application to the surf zone," *Ocean Modelling*, vol. 34, pp. 16–35, 2010.

[26] D. J. R. Walstra, J. Roelvink, and J. Groeneweg, "Calculation of wave-driven currents in a 3D mean flow model," in *Proceedings of the 27th international conference on coastal engineering, Sydney*, vol. 2. ASCE, 2000, pp. 1050–1063.

[27] J. A. Battjes, "Modelling of turbulence in surf zone," in *Symposium on Modelling Techniques, San Francisco*. ASCE, 1975, pp. 1050–1061.

[28] J. Smagorinsky, "General circulations experiments with the primitive equations i. the basic experiment," *Monthly Weather Review*, vol. 8, pp. 99–165, 1963.